nature nanotechnology

SUPPLEMENTARY INFORMATION

DOI: 10.1038/s41565-017-0001-2

In the format provided by the authors and unedited.

Electric polarization switching in an atomically thin binary rock salt structure

Jose Martinez-Castro[1,2,3,9], Marten Piantek[3,4,5], Sonja Schubert[3,5], Mats Persson[6,7], David Serrate[3,4,5]* and Cyrus F. Hirjibehedin[1,2,8]*

[1]London Centre for Nanotechnology, University College London (UCL), London WC1H 0AH, UK. [2]Department of Physics & Astronomy, UCL, London WC1E 6BT,
UK. [3]Instituto de Nanociencia de Aragón and Laboratorio de Microscopías Avanzadas, Universidad de Zaragoza, 50018 Zaragoza, Spain. [4]Fundación Instituto de Nanociencia de Aragón (FINA), 50018 Zaragoza, Spain. [5]Departamento de Física de la Materia Condensada, Universidad de Zaragoza, 50009 Zaragoza, Spain. [6]Surface Science Research Centre and Department of Chemistry, University of Liverpool, Liverpool L69 3BX, UK. [7]Department of Physics, Chalmers University of Technology, SE-412 96 Göteborg, Sweden. [8]Department of Chemistry, UCL, London WC1H 0AJ, UK. Present address: [9]Department of Quantum Matter Physics, University of Geneva, CH-1211 Geneva 4, Switzerland. *e-mail: serrate@unizar.es; c.hirjibehedin@ucl.ac.uk

Electric polarisation switching in an atomically-thin binary rock salt structure

Jose Martinez-Castro, Marten Piantek, Sonja Schubert, Mats Persson, David Serrate, and Cyrus F. Hirjibehedin

Supplementary Methods

Scanning Tunnelling Microscopy and Atomic Force Microscopy

Scanning tunnelling microscopy (STM) experiments were performed using a Specs JT-STM, a commercial adaptation of the design described by Zhang *et al.* [1]; STM and atomic force microscopy (AFM) experiments were performed using an Omicron Nanotechnology LT-STM with a qPlus force sensor [2] installed for combined STM/AFM operation. Both systems were operated in ultrahigh vacuum conditions, with typical chamber pressures below 2×10^{-10} mbar, and at base temperatures of 1.1 K and 4.5 K respectively.

The bias voltage V is always quoted in sample bias convention. Topographic images were obtained in the constant current imaging mode with V and tunnel current I set to V_{set} and I_{set} respectively. For areas with NaCl bilayer on Cu_2N/Cu(001), stable constant current images at positive bias could not be obtained. For bias voltages that produce electric fields close to the critical switching field, the vertical motion of the tip during topographic imaging results in large variations in the tunnelling current, which cannot be stabilised by the feedback loop. Increasing the electric field to be large enough that such switching does not occur during image acquisition requires moving the tip closer to the surface, which then causes damage to the tip and/or surface. Applying larger bias voltages near or above the Cu_2N conduction band edge (~2.1 eV) [3], causes a large retraction of the tip owing to the Cu_2N contribution to the tunnelling current, which decreases the electric field below the critical value. I vs Δz (and Δf vs Δz) measurements were obtained by initially setting V=V_{set} and I=I_{set}, disabling the feedback loop, setting V to its final value for the measurement, and then recording I (and Δf) while changing Δz.

The qPlus sensor with a resonance frequency of f_0 = 23379.5 Hz and a stiffness $k \sim 1800$ N/m [4] was operated in non-contact AFM mode with a phase-locked excitation at a constant oscillation amplitude of A = 20 pm. The intrinsic energy loss per oscillation cycle ΔE_{TF} = 0.7 meV has been estimated by the ratio of the tuning fork's energy $E = k/2\ A^2$ and its quality factor Q = 20150 [4]. The relative change of the dissipation $(\Delta E_{TF} + \Delta E_{TS})/\Delta E_{TF}$ due to additional non-conservative tip-sample interactions was calculated from the ratio (g'/g) with g and g' being the gains of the amplitude regulation for the free and the interacting qPlus sensors, respectively.

Cu(001) samples (MaTeck single crystal with 99.999% purity) were prepared by repeated cycles of sputtering and annealing with Ar and annealing to 500 ˚C. Cu_2N is prepared on top of clean Cu(001) samples by sputtering with N_2 and annealing to 350 ˚C [5]. Evaporation of NaCl was performed using a Knudsen effusion cell operated at 590 ˚C and with the Cu_2N/Cu(001) substrate held at room temperature. Our studies indicate that bilayers of NaCl can be formed on both bare Cu(001) and the Cu_2N/Cu(001) irrespective of the Cu_2N surface coverage, while a NaCl monolayer is stabilised only on top of Cu_2N, or above the atomically narrow Cu trenches between closely spaced Cu_2N islands.

Topographic images obtained using STM were processed using WSxM [6].

Density Functional Theory

The electronic and geometric structure of NaCl on Cu_2N/Cu(001) was investigated by density functional theory (DFT) calculations using the Vienna ab-initio simulation program (VASP) [7]. The electron-ion-core interactions and the exchange-correlation effects were treated using the projected augmented wave (PAW) method [8] with a plane-wave, kinetic energy cut-off of 400 eV, and the optB86b version of the van der Waals density functional [9-12], respectively. The system was represented in a super-cell by a six layer Cu(001) slab with a two Cu atoms in each layer and a 18.6 Å vacuum region. The Brilliouin zone was sampled by a 12x12x1 *k*-point grid. During the geometry optimisation, the atoms in the bottom two layers were constrained at their bulk positions with the bulk lattice constant *a* of 3.60 Å (the calculated value for bulk Cu) and *a* = 3.72 Å (the observed value for Cu_2N), and consistent results were obtained in both cases. All presented results are based on *a* = 3.60 Å. The positions of the remaining atoms were relaxed until all forces were less than 0.02 eV $Å^{-1}$. The electric field was introduced in the calculations using the method described in Ref. 12.

Supplementary Figures and Tables

a = 3.60 Å			
	N Site	Cl Site	Hollow Site
E_f (eV)	-2.00	-2.07	-2.19
ΔE_f (eV)	0.19	0.12	0.00
E_{ad} (eV)	-0.18	-0.25	-0.36
a = 3.72 Å			
E_f (eV)	-2.10	-2.19	-2.33
ΔE_f (eV)	0.23	0.14	0.00
E_{ad} (eV)	-0.18	-0.26	-0.40

Supplementary Table 1 – NaCl on Cu_2N formation and adsorption energy. Calculated film formation energy E_f (per NaCl dimer), relative change in film formation energy ΔE_f, and film adsorption energies E_{ad} in the surface unit cell. Values are shown for lattice constants a = 3.60 Å (the calculated value for bulk Cu) and a = 3.72 Å (the observed value for Cu_2N).

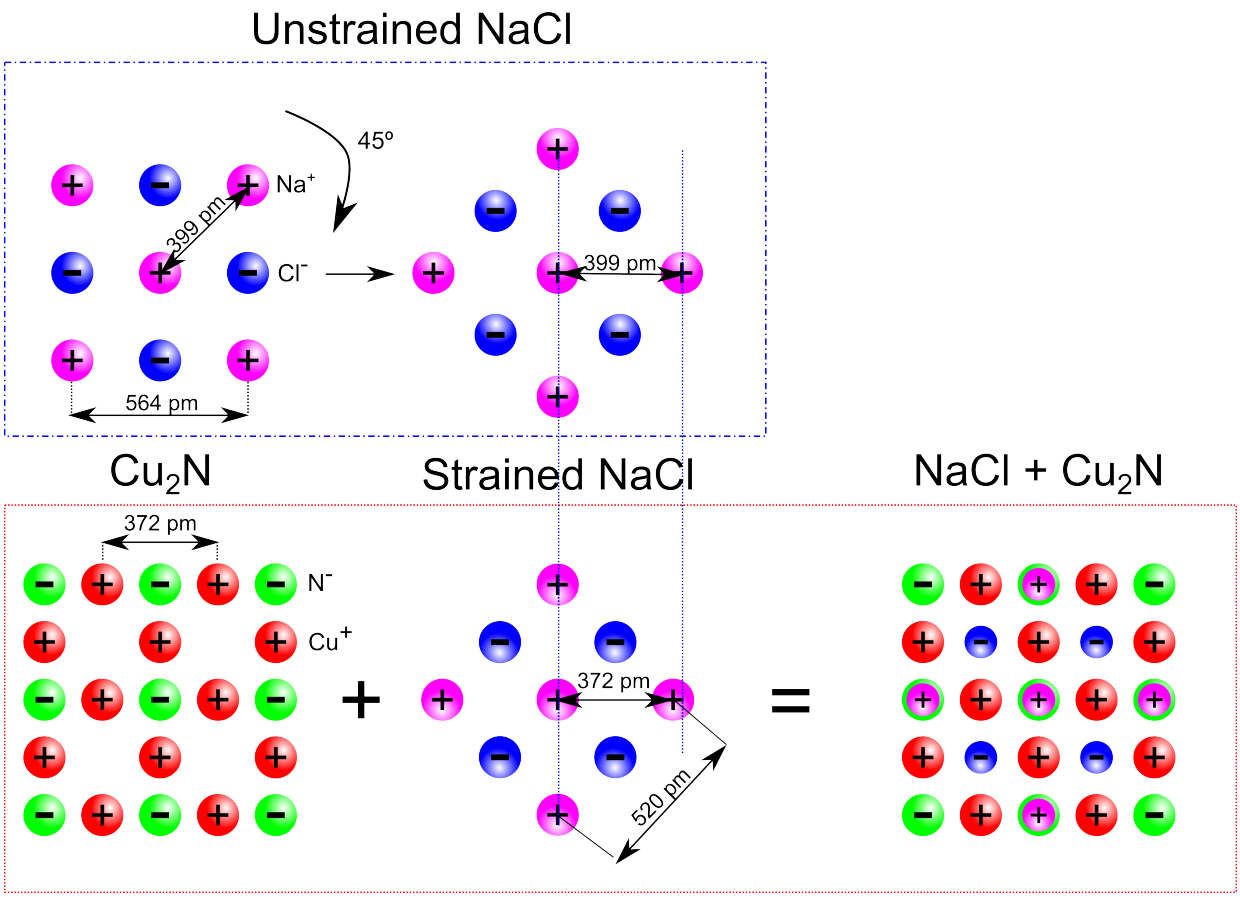

Supplementary Figure 1 – Binding geometry of NaCl on Cu_2N. Upper illustration shows the (001) surface termination of NaCl with Na (purple) and Cl (blue) atoms in an unstrained configuration in two different orientations. Lower illustration shows the (001) surface termination of Cu (red) and N (green) atoms in a Cu_2N layer and an NaCl layer, whose lattice constant can be made to match that of the Cu_2N if it is strained by 7%.

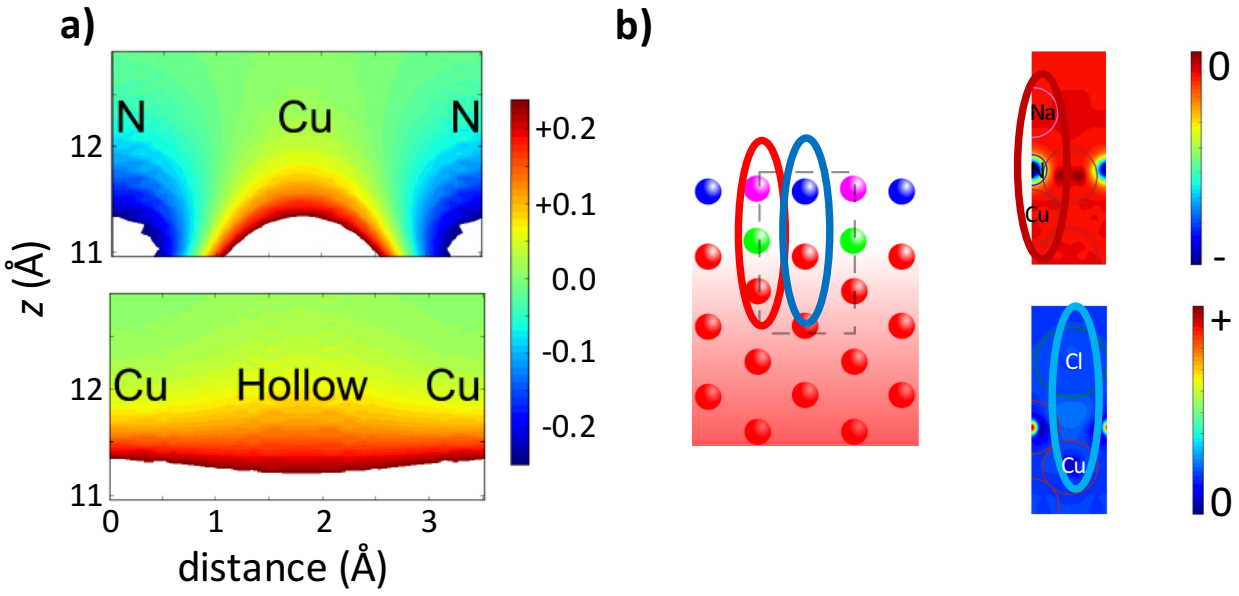

Supplementary Figure 2 – Bonding between NaCl and Cu_2N single atomically thin layers. a) Calculated electrostatic potential (in units of V) above Cu_2N/Cu(001) for the structure corresponding to the relaxed configuration with an adsorbed NaCl monolayer and a Cu lattice parameter of 3.60 Å. The potential is negative (blue) above the N site and positive (red) above the Cu and Hollow sites. b) Calculated electron density difference between the NaCl/Cu_2N/Cu(001) heterostructure and the isolated NaCl and Cu_2N/Cu(001) in the same relaxed configuration as for the heterostructure. Although some electron rearrangements are observed between the Cu and N atoms in the Cu_2N layer, no significant electron rearrangements are observed between NaCl and Cu_2N layers, indicating a purely electrostatic bonding between these atomically thin layers.

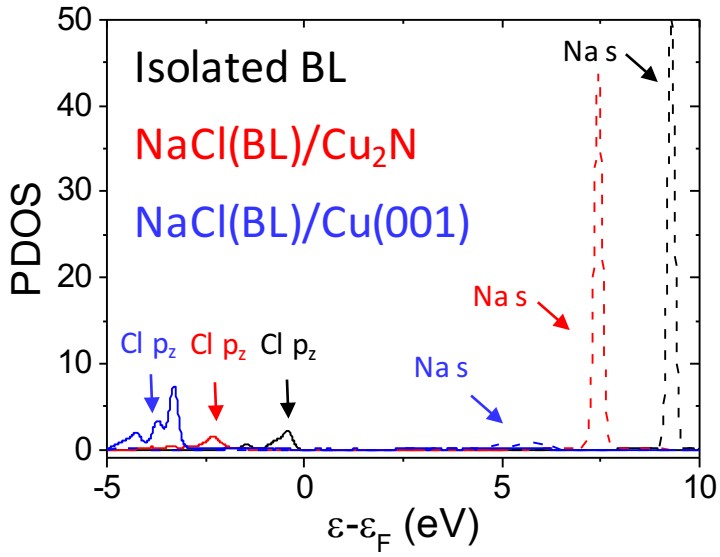

Supplementary Figure 3 – Partial density of states (PDOS) for isolated and adsorbed NaCl. PDOS of isolated NaCl bilayer (black) with 0.2 eV broadening, showing the Cl(p_z) (solid lines) and Na(s) (dashed lines) states, along with PDOS for NaCl bilayer on Cu_2N/Cu(001) (red) and NaCl bilayer on Cu(001) (blue). The Fermi level ε_F of NaCl bilayer on Cu_2N/Cu(001) and on Cu(001) is the energy of the highest occupied state of the isolated film. Despite being adsorbed on the surface, the NaCl states remain sharp with the Cu_2N spacer over the metal. However, for NaCl bilayer on Cu(001), the NaCl states are broadened significantly, indicating a mixing of the NaCl states with the metal states.

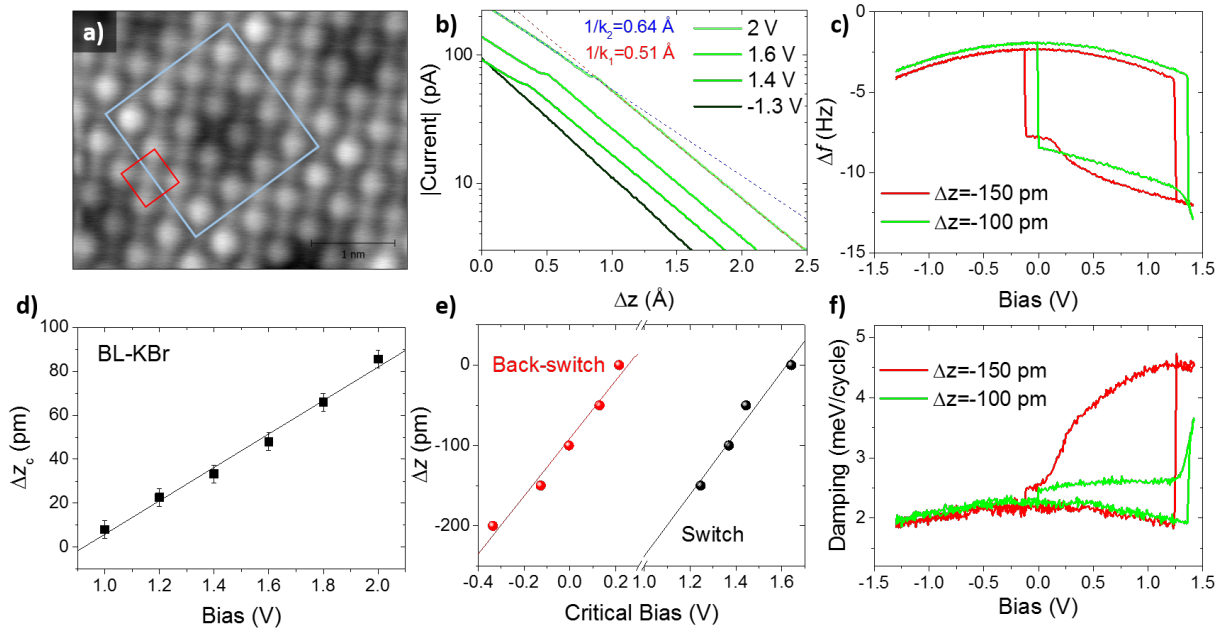

Supplementary Figure 4 – Electric field induced switching for KBr bilayer on $Cu_2N/Cu(001)$. a) STM topography of KBr bilayer (V_{set}=-1.3 V, I_{set}=30 pA, 3×4 nm). In contrast to NaCl, KBr keeps its own lattice parameter, giving rise to rotational Moirée patterns. This topography represents the most common pattern; the red and light blue squares are the surface unit cell of KBr and the Moirée unit cell. b) *I* vs. *Δ*z acquired over the KBr bilayer. Black to green colour code represents the curves taken at bias voltages increasing from -1.3 V to 2 V. Two regimes with characteristic exponential decay lengths $1/k_{1(2)}$ are observed: (i) small $1/k_1$ (red exponential trend) for V<1 V (or high work function); (ii) higher $1/k_2$ (blue exponential trend) for V≥1 V and tip-sample distance below a critical Δz_c value (or low workfunction). As in the case of NaCl bilayer, these regimes correspond to two different values of the surface polarisation. Δz=0 is defined by V_{set}=-1.3 V, I_{set}=100 pA. c) $\Delta f(V)$ measurements above a different position of the KBr bilayer Moirée pattern for various tip displacements (V_{set}=-1.3 V, I_{set}=0.9 pA). The Kelvin probe parabola of the original state is clearly visible. For sample bias above a critical value V_{C1}, an abrupt switch to another state with larger attractive electrostatic force takes place. The bilayer KBr switches back to the original stage while reversing the applied electric field at a lower critical value V_{C2}, indicating strong hysteretic behaviour of the polarisation in this sample area. Note that, in contrast to NaCl bilayer, the presence of anion vacancies is not required to observe strong hysteresis in KBr bilayer. d) Linear variation of Δz_C as a function of applied bias extracted from panel (b). The slope corresponds to a critical electric field of E_C=13 GV/m. (e) Linear variation of Δz as a function of $V_{C1(2)}$ obtained from the data in panel (c). In this case, the best linear fit yields E_C=2.7 GV/m. Note that back-switching is observed at both positive and negative applied voltages. This is likely because of an additional intrinsic offset voltage arising from the contact potential difference between the tip and substrate. The offset can be tuned by changing the work functions of either or both electrodes, by using different materials or by inducing a different atomic configuration for the tip apex. f) Dissipation channel simultaneously recorded with $\Delta f(V)$ from panel c. As in the case of NaCl, when the electrostatic force jumps following the switch of the surface polarisation, the dissipation steeply increases/decreases as corresponds to a non-reversible interaction during the oscillation cycle. While the polarisation remains in the high field state (bias is ramped from a value larger than V_{C1} to a value larger than V_{C2}) the associated structural deformation enhances the coupling between the surface atoms and the tip's oscillation, resulting in larger dissipation than in the low field state.

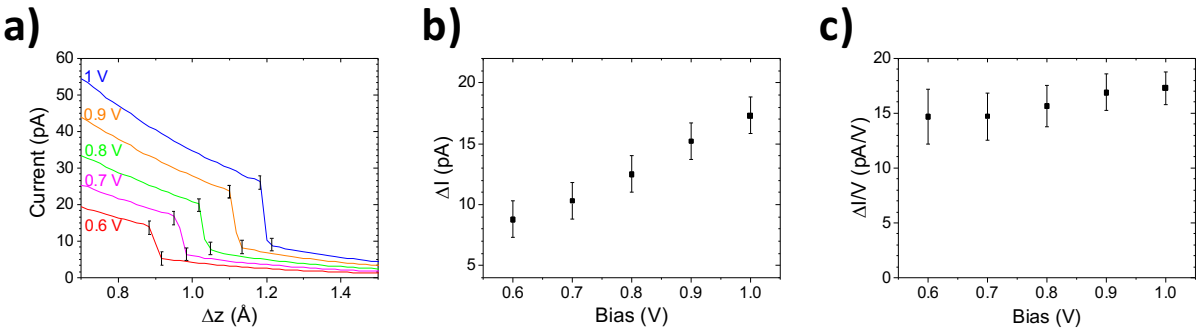

Supplementary Figure 5 – Scaling of current step with voltage. a) I vs Δz acquired above the NaCl bilayer on $Cu_2N/Cu(001)$ (V_{set}=-1.3 V, I_{set}=200 pA); some data are also shown in Fig. 2a. Vertical black lines label the two different current states on each trace. b) Change in current between the two states ΔI vs V. Vertical error bars are determined by extending the uncertainty of the transition to the next three acquired data points. c) Change in conductance $\Delta I/V$ vs V, which is seen to be approximately constant with V as expected for a change between two distinct work functions in the tunnel barrier.

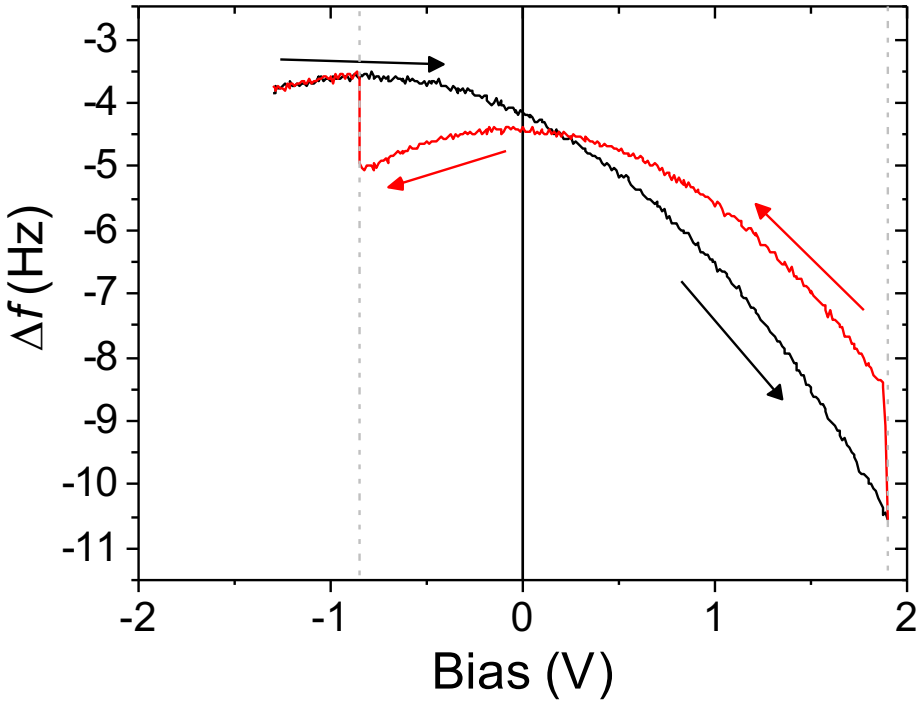

Supplementary Figure 6. **Hysteretic reversal of the polarisation in the proximity of a vacancy**. *Δf(V)* measurements above a Cl^- anion close to a vacancy for V_{set}=-1.3 V, I_{set}=10 pA. Two states are distinguished: a self-poled state (black) and a switched state (red). A strong change of the polarisation is noticed through the change in the V_{cpd} between both states. Grey dashed lines indicate the critical bias for the reversal of the polarisation. Although the Cl^- vacancy stabilizes the switched state, the strong self-poling of NaCl shifts the whole cycle to positive electric fields.

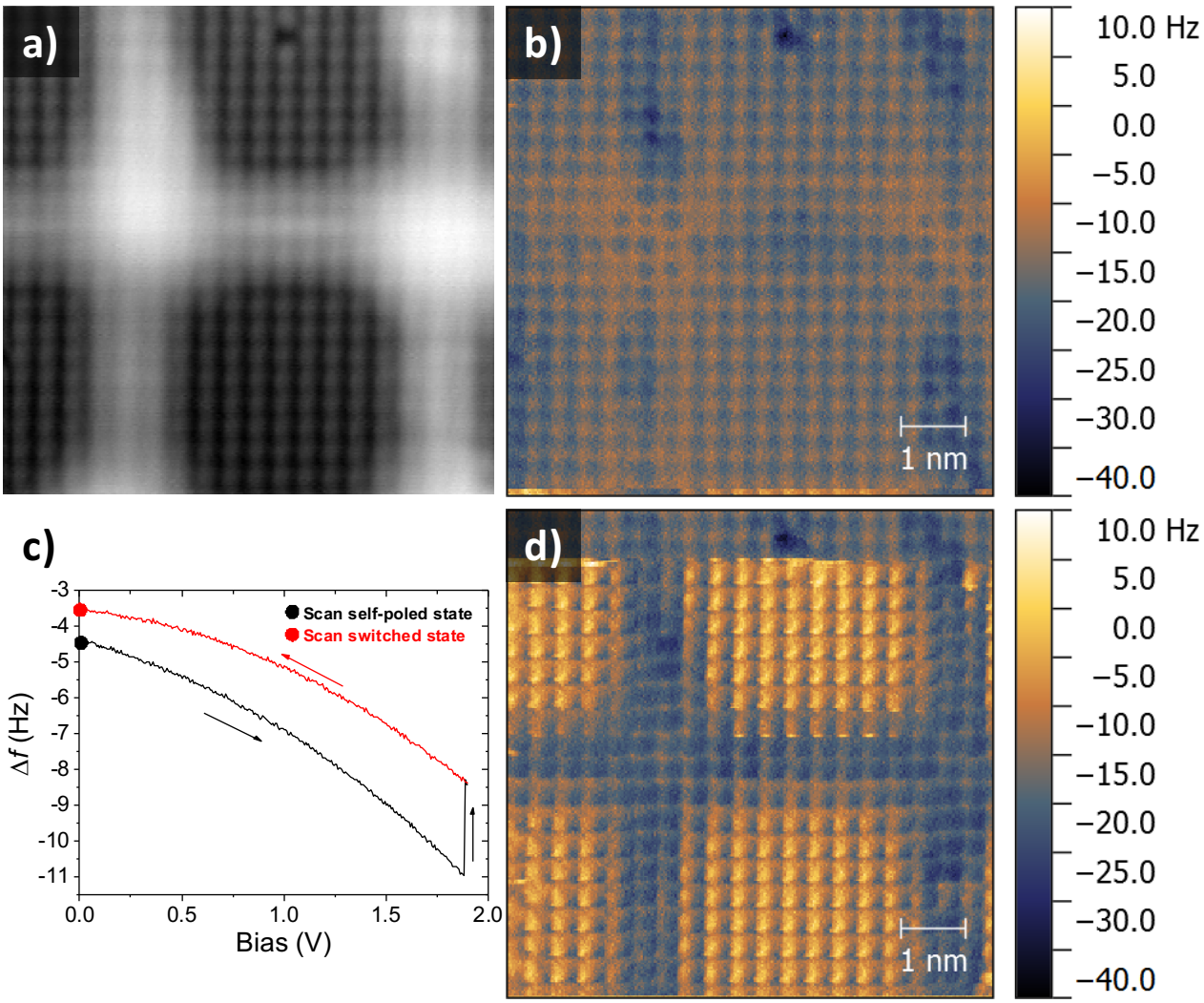

Supplementary Figure 7 – Spatial extension of the reversed polarisation measured by constant height Δ*f* means.

a) Topographic STM image of a Cu(001) surface mostly covered by Cu_2N islands with small stripes of Cu in between with NaCl bilayer on top. A Cl^- vacancy can be observed in the upper part of the image. b) Constant height image of Δ*f*. The image was taken as follows: from the regulation conditions V_{set}=-1.3 V and I_{set}=10 pA, the feedback was opened. The bias was then set to zero (V_{set}=0 V). To have sufficient resolution in the Δ*f* signal, the tip was approached (Δ*z*=-2.1 Å) and then imaging was performed. c) Part of a polarisation inversion cycle performed above a Cl anion close to a vacancy. After scanning the sample at the given conditions mentioned in b), the tip was retracted to its original height (Δ*z*=0 Å) and Δ*f*(*V*) was recorded so as to reverse the polarisation (V_c=1.89 V) leaving the bias again at V_{set}=0. d) After the bias cycle described in c), the tip was placed at the beginning of the frame scan and approached Δ*z*=-2.1 Å before beginning the scan. The contrast change in Δ*f* indicates a stronger interaction between the tip and the switched state compared to the self-poled state. Although the total extension of the switched state cannot be resolved, it is possible to see that the switched state crosses different Cu_2N islands. When the tip rescans the area near the vacancy at the low vertical distance, the surface switches back to the self-poled state.

Supplementary Discussion

Formation and adsorption energies of NaCl on Cu_2N

The formation energy of n monolayers (nML) per NaCl dimer is defined here as

$$E_f = [E(\mathrm{NaCl}(n\mathrm{ML})/\mathrm{Cu_2N}/\mathrm{Cu}(001)) - E(\mathrm{Cu_2N}/\mathrm{Cu}(001)) \; - n\,E(\mathrm{NaCl})]/n$$

where $E(\mathrm{NaCl})$ is the energy of an isolated NaCl dimer.

The film adsorption energy in the surface unit cell is defined as:

$$E_{ad} = E(\mathrm{NaCl}(n\mathrm{ML})/\mathrm{Cu_2N}/\mathrm{Cu}(001)) - E(\mathrm{Cu_2N}/\mathrm{Cu}(001)) \; - \; E(\mathrm{NaCl}(n\mathrm{ML}))$$

Three adsorption sites are considered, with Cl above the N site, Cu site and Hollow site in the Cu_2N. A fourth (Bridge) site was found to be unstable and relaxed into the Hollow site configuration during structural optimisation. As seen in Supplementary Table 1, the formation and adsorption energies are minimised when Cl is on top of hollow site, making it the most favourable binding arrangement. Furthermore, this conclusion is not sensitive to the precise value chosen for the lattice constant a.

Supplementary References

[1] Zhang, L., Miyamachi, T., Tomanic, T., Dehm, R. & Wulfhekel, W. A compact sub-Kelvin ultrahigh vacuum scanning tunneling microscope with high energy resolution and high stability. *Rev. Sci. Instrum.* **82**, 103702 (2011)
[2] Giessibl, F. J. High-speed force sensor for force microscopy and profilometry utilizing a quartz tuning fork. *Appl. Phys. Lett.* **73**, 3956-3958 (1998)
[3] Ruggiero C. D., Choi T. and Gupta J. A. Tunneling spectroscopy of ultrathin insulating films: CuN on Cu(001). *Appl. Phys. Lett.* **91**, 253106 (2007)
[4] Giessibl, F .J. Advances in atomic force microscopy. *Rev. Mod. Phys.* 75, 949-983 (2003)
[5] Leibsle, F. M., Dhesi, S. S., Barrett, S. D. & Robinson, A. W. STM observations of Cu(100)−c(2×2)N surfaces: evidence for attractive interactions and an incommensurate c(2×2) structure. *Surf. Sci.* **317**, 309-320 (1994)
[6] Horcas, I. *et al.* WSXM: A software for scanning probe microscopy and a tool for nanotechnology. *Rev. Sci. Inst.* **78**, 013705 (2007).
[7] Kresse, G. & Joubert, D. From ultrasoft pseudopotentials to the projector augmented-wave method. *Phys. Rev. B* **59**, 1758-1775 (1999).
[8] Blöchl, P. E. Projector augmented-wave method. *Phys. Rev. B* **50**, 17953-17978 (1994).
[9] Dion, M., Rydberg, H., Schröder, E., Langreth, D. C. & Lundqvist, B. I. Van der Waals Density Functional for General Geometries. *Phys. Rev. Lett.* **92**, 246401 (2004).
[10] Thonhauser, T. *et al.* Van der Waals density functional: Self-consistent potential and the nature of the van der Waals bond. *Phys. Rev. B* 76, 125112 (2007).
[11] Román-Pérez, G. & Soler, J. M. Efficient implementation of a van der Waals density functional: application to double-wall carbon nanotubes. *Phys. Rev. Lett.* 103, 096102 (2009).
[12] Klimes, J., Bowler, D. R. & Michaelides, A. Van der Waals density functionals applied to solids. *Phys. Rev. B* 83, 195131 (2011).
[13] Scivetti, I. & Persson, M. A simplified density functional theory method for investigating charged adsorbates on an ultrathin, insulating film supported by a metal substrate. *J. Phys. Condens. Matter* 26, 135003 (2014).